Immersed domain approach for fluid-structure-contact interaction

FEM@LLNL Seminar Series (`https://mfem.org/seminar`)

Patrick Zulian[1,2], Maria Nestola[2], Fabian Wermelinger[3], Luca Mangani[3], Rolf Krause[1,2,5]

(**Acknowledgements** || **HPC**: Simone Riva[2] | **Preconditioners**: Hardik Kothari[1,2], Panayot Vassilevski[6], Austen Nelson[6] | **FSI**: Alexander Masero[3], Mahdi Mhamad Alloush[3], Ernesto Casartelli[3]
Pumps: Raphael Frey[4], Michael Gnos[4], Marcel Holzman[4], Stephan Kaufmann[4], Christian Widmer[4] **BHV**: Dominik Obrist[7], Barna Becsek[7], Pascal Corso[8])

1. **UniDistance Suisse**, Brig, Switzerland.
2. **Euler Institute**, Università della Svizzera italiana, Lugano, Switzerland.
3. **HSLU**, Lucerne, Switzerland. 4. **KNF Flodos AG**, Sursee, Switzerland.
5. **KAUST**, Thuwal, Saudi Arabia.
6. **Portland State University**, Orgeon, USA.
7. **UniBe**, Bern, CH. 8. **ETHZ**, Zurich, CH.

Tuesday, February 18th, 9AM PDT / 18PM CET, LLNL, Virtual

Flow (and transport) in fractured porous media

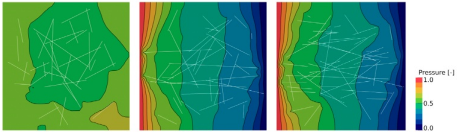

Contact

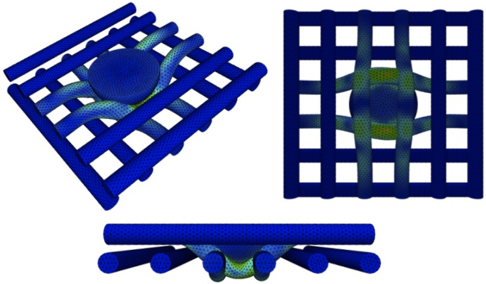

Fluid-structure interaction (Video)

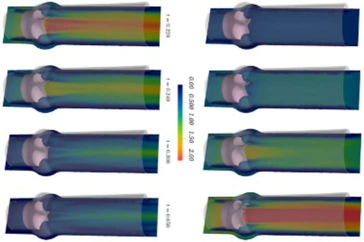

Types of discrete fractures

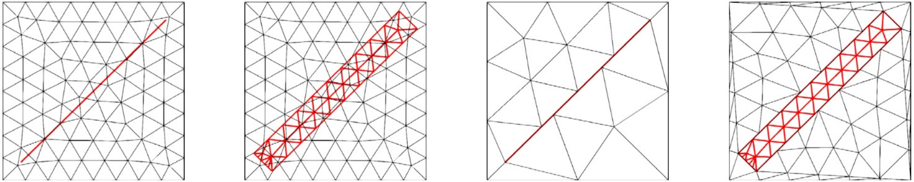

(a) Embedded-HD (b) Embedded-ED (c) Decomposition-HD (d) Decomposition-ED

Embedded/Immersed

- Fracture network mesh is independent from matrix mesh
- Convenient for stochastically generated and complex networks
- Intersections and coupling of discrete fields

Fitted/Decomposition

- Exact representation of interface in matrix
- Complexity in meshing stage
- High-resolution meshes vs ill-shaped elements

Flow in fractured porous media

- Matrix domain $\Omega \subset \mathbb{R}^d, d \in \{2, 3\}$
- Fracture $\subset \Omega$ (manifold dim. d or $d-1$)
- Pressure p, p
- Sink/source f, f
- Lagrange multiplier
- Permeability $\boldsymbol{K}, \boldsymbol{K}$

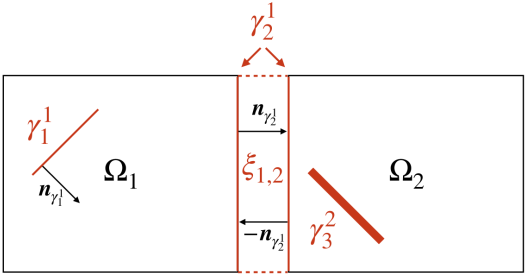

The weak form: find $(p, p \quad) \in V$ and $\quad \in \quad$, such that

$$
\begin{aligned}
(\boldsymbol{K}\nabla p, \nabla q)_\Omega - (\quad , q) \quad &= (f, q)_\Omega, \\
(\boldsymbol{K} \quad \nabla p \quad , \nabla q \quad) \quad + (\quad , q \quad) \quad &= (f \quad , q \quad) \quad ,
\end{aligned}
$$

and the weak equality condition $-(p - p \quad , \quad) \quad = 0$, are satisfied, $\forall (q, q \quad) \in W$, and $\forall \quad \in$

Flow in fractured porous media: discretization

- Finite element method
- Meshes $\mathscr{M}_i = \mathscr{M}_{\Omega_i}$ for the matrix sub-domains $\Omega_i, i = 1, \ldots N$
- Meshes $\mathscr{M}_{\ \ k}$ for fractures $\ \ _k, k = 1 \ldots N$
- Multiplier space on fracture, we set $\mathscr{M}_{\ \ k} = \mathscr{M}_{\ \ k}$
- Lagrange elements $\mathbb{P}^k$, or tensor-product elements $\mathbb{Q}^k$ of order k

$$
\begin{aligned}
W_{h,\ } = \{ w \in W(\ \ ) : \forall E \in \mathscr{M}_{\ } \ ,\\
w|_E \in \left\{ \begin{array}{ll} \mathbb{P}^k & \text{if } E \text{ is a simplex} \\ \mathbb{Q}^k & \text{if } E \text{ is a hyper-cuboid} \end{array} \right\} \\
\}, \\
\ \in \{\Omega, \ \ ^d, \ \ ^{d-1}\}, \\
\ _{h,} \qquad \ \in \{\ \ ^d, \ \ ^{d-1}\} \quad \text{(Lagrange multiplier space)}
\end{aligned}
$$

- $\{\ \ _i\}_{i\in J}$ is the basis of $W_{h,\Omega}$
- $\{\ \ _j\}_{j\in J}$ is the basis of $W_{h,}$
- $\{\ \ _k\}_{k\in J}$ is the basis of $\ \ _h$
- J and $J\ \ \subset \mathbb{N}$ are nodes index sets
- Function $p \in W_{h,\Omega}$, $p\ \ \in W_{h,}$, and $\ \ \in\ \ _{h,}$
- $p = \sum_{i\in J} p_i\ \ _i$
- $p\ \ = \sum_{j\in J}\ p_j\ \ _j$
- $\ \ = \sum_{k\in J}\ \ _k\ \ _k$
- $(\ \ _i,\ \ _j)_{\ \ h} =\ \ _{ij}(\ \ _i, 1)_{\ \ h} \qquad \forall i, j \in J$ (**bi-orthogonality**)
- $(\ \ _j, 1)_{\ \ h} > 0$ (**positivity**)

Point-wise algebraic equations

- Porous matrix ($\mathbf{A}\mathbf{p} - \mathbf{B}^T\boldsymbol{\lambda} = \mathbf{f}$)

$$\sum_{i\in J} p_i(\mathbf{K}\nabla\ \ _i, \nabla\ \ _j)_{\Omega_h} - \sum_{k\in J}\ \ _k(\ \ _k,\ \ _j)_{\ \ h} = (f,\ \ _j)_{\Omega_h}, \qquad \forall j \in J,$$

- Fracture ($\mathbf{A}\ \ \mathbf{p}\ \ + \mathbf{D}^T\boldsymbol{\lambda} = \mathbf{f}\ \ $)

$$\sum_{i\in J} p_{i,}\ (\mathbf{K}\ \ \nabla\ \ _i, \nabla\ \ _j)_{\ \ h} + \sum_{k\in J}\ \ _k(\ \ _k,\ \ _j)_{\ \ h} = (f\ \ ,\ \ _j)_{\ \ h}, \qquad \forall j \in J\ \ ,$$

- Weak-equality condition ($-\mathbf{B}\mathbf{p} + \mathbf{D}\mathbf{p}\ \ = \mathbf{0}$)

$$-\left(\sum_{i\in J} p_i(\ \ _i,\ \ _j)_{\Omega_h} - \sum_{k\in J} p_{k,}\ (\ \ _k,\ \ _j)_{\ \ h}\right) = 0, \qquad \forall j \in J$$

Linear system of equations

- Saddle-point system

$$\begin{vmatrix} \mathbf{A} & \mathbf{0} & -\mathbf{B}^T \\ \mathbf{0} & \mathbf{A} & \mathbf{D}^T \\ -\mathbf{B} & \mathbf{D} & \mathbf{0} \end{vmatrix} \begin{vmatrix} \mathbf{p} \\ \mathbf{p} \\ \boldsymbol{\lambda} \end{vmatrix} = \begin{vmatrix} \mathbf{f} \\ \mathbf{f} \\ \mathbf{0} \end{vmatrix}$$

- Gaussian-elimination → condensed system

$$(\mathbf{A} + \mathbf{T}^T \mathbf{A}\ \ \mathbf{T})\mathbf{p} = \mathbf{f} + \mathbf{T}^T \mathbf{f}\ ,$$

- $\mathbf{T} = \mathbf{D}^{-1}\mathbf{B}$
- **D** is trivially invertible thanks to bi-orthogonal basis
- Symmetric-positive definite linear system solved only for **p**
- Solved with preconditioned CG or AMG (e.g., Hypre)

Handling non-conforming meshes → computing $\mathbf{T} = \mathbf{D}^{-1}\mathbf{B}$

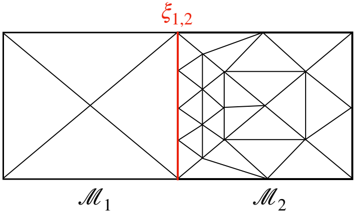

(a) Non conforming interface $_{1,2}$ between mesh $\mathcal{M}_1$ and mesh $\mathcal{M}_2$.

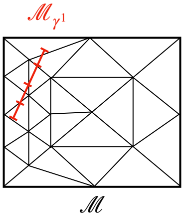

(b) Meshes for fracture $\mathcal{M}_1$ and porous matrix $\mathcal{M}$ for the embedded scenario.

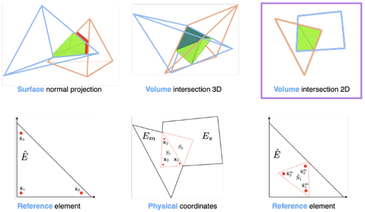

(c) Numerical quadrature within intersections

Matrix (mortar)	Fracture (nonmortar)	Intersection type
$\Omega \subset \mathbb{R}^3$	3	polyhedron-polyhedron
$\Omega \subset \mathbb{R}^3$	2	polyhedron-polygon
$\partial\Omega_i \cap \;_{i,j} \subset \mathbb{R}^3$	$\partial\Omega_j \cap \;_{i,j} \subset \mathbb{R}^3$ 2	polygon-polygon (oriented)
$\Omega \subset \mathbb{R}^2$		polygon-polygon
$\Omega \subset \mathbb{R}^2$	1	polygon-segment
$\partial\Omega_i \cap \;_{i,j} \subset \mathbb{R}^2$	$\partial\Omega_j \cap \;_{i,j} \subset \mathbb{R}^2$	segment-segment (oriented)

Results are selected from these contributions

3D non-conforming mesh model for flow in fractured porous media using Lagrange multipliers (Schädle, Zulian, Vogler, Bhopalam, Nestola, Ebigbo, Krause, and Saar [2019])

Contents lists available at ScienceDirect
Computers and Geosciences
journal homepage: www.elsevier.com/locate/cageo
ELSEVIER

Research paper

3D non-conforming mesh model for flow in fractured porous media using Lagrange multipliers[☆,☆☆]

Philipp Schädle[a,*], Patrick Zulian[b], Daniel Vogler[a], Sthavishtha R. Bhopalam[a], Maria G.C. Nestola[b], Anozie Ebigbo[a], Rolf Krause[b], Martin O. Saar[a]
[a] ETH Zürich, Geothermal Energy and Geofluids Group, Institute of Geophysics, 8092 Zürich, Switzerland
[b] USI Lugano, Institute of Computational Science, 6904 Lugano, Switzerland

ARTICLE INFO

Keywords:
Embedded discrete fracture model
Flow in 3D fractured porous media
Finite element method
Non-conforming grids

ABSTRACT

This work presents a modeling approach for single-phase flow in 3D fractured porous media with non-conforming meshes. To this end, a Lagrange multiplier method is combined with a parallel variational transfer approach. This Lagrange multiplier method enables the use of non-conforming meshes and depicts the variable coupling between fracture and matrix domain. The variational transfer allows general, accurate, and parallel projection of variables between non-conforming meshes (i.e. between fracture and matrix domain). Comparisons of simulations with 2D benchmarks show good agreement, and the applied finite element Lagrange multiplier spaces show good performance. The method is further evaluated on 3D fracture networks by comparing it to results from conforming mesh simulations which were used as a reference. Application to realistic fracture networks with hundreds of fractures is demonstrated. Mesh size and mesh convergence are investigated for benchmark cases and 3D fracture network applications. Results demonstrate that the Lagrange multiplier method, in combination with the variational transfer approach, is capable of modeling single-phase flow through realistic 3D fracture networks.

Comparison and application of non-conforming mesh models for flow in fractured porous media using dual Lagrange multipliers (Zulian, Schädle, Karagyaur, and Nestola [2020])

Contents lists available at ScienceDirect
Journal of Computational Physics
www.elsevier.com/locate/jcp
ELSEVIER

Comparison and application of non-conforming mesh models for flow in fractured porous media using dual Lagrange multipliers[☆]

Patrick Zulian[a,*], Philipp Schädle[b], Liudmila Karagyaur[a], Maria G.C. Nestola[a,c]
[a] Euler institute, USI Lugano, 6900 Lugano, Switzerland
[b] Institute of Geophysics, Department of Earth Sciences, ETH Zürich, 8092 Zürich, Switzerland
[c] Institute of Geochemistry and Petrology, Department of Earth Sciences, ETH Zürich, 8092 Zürich, Switzerland

ARTICLE INFO

Article history:
Available online 18 October 2021

Keywords:
Discrete fracture model
Non-matching meshes
Flow in fractured porous media
Finite element method
Non-conforming meshes
Lagrange multiplier method

ABSTRACT

Geological settings, such as reservoirs, include fractures with different material properties and geometric features. Hence, numerical simulations in applied geophysics demands for computational frameworks which efficiently allow us to integrate various fracture geometries in a porous medium matrix. This study focuses on a modeling approach for single-phase flow in fractured porous media and its application to different types of non-conforming mesh models. We propose a combination of the Lagrange multiplier method with variational transfer techniques for simulating flow through fractured porous media by employing complex non-conforming geometries as well as hybrid- and equi-dimensional models and discretizations. The variational transfer is based on the L^2-projection and enables an accurate and highly efficient parallel projection of fields between non-conforming meshes (e.g., between fracture and porous matrix domain).

We present the different techniques as a unified mathematical framework with a practical perspective. By means of numerical examples we discuss both, performance and applicability of the particular strategies. Comparisons of finite element simulation results to widely adopted 2D benchmark cases show good agreement and the dual Lagrange multiplier spaces show good performance. In an extension to 3D fracture network, we first provide complementary results to a recently developed benchmark case and afterwards we explore a complex scenario which leverages the different types of fracture meshes. Complex and highly conductive fracture networks are found more suitable in combination with embedded hybrid-dimensional fractures. However, thick and blocking fractures are better approximated by equi-dimensional embedded fractures and the equi-dimensional mortar method, respectively.

Benchmark 1: regular fracture network

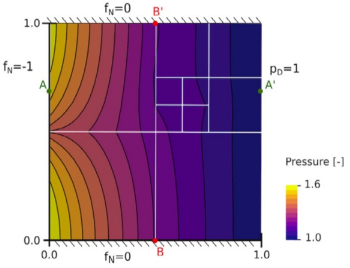

(a) Embedded/conductive

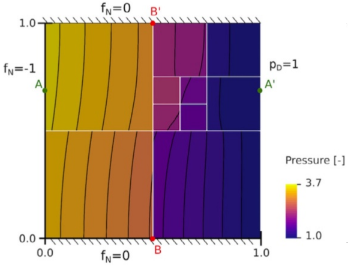

(b) Decomposition/blocking

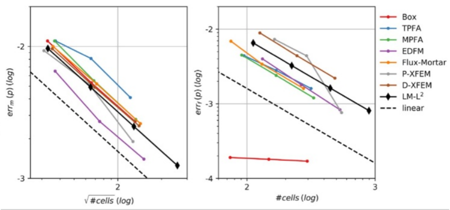

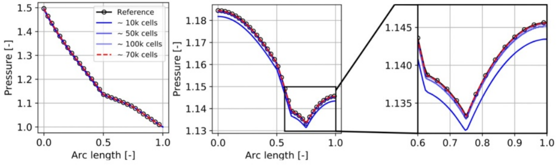

A A' **B B'**

Method	#-matr.	#-frac.	d.o.f.	nnz/size^2	$\|\cdot\|_2$-cond.	err_m
Embedded-ED	10 656 triangles	8648	5853	2.6e-4	3.7e6	3.3e-5
Embedded-ED	47 142 triangles	8648	25 992	7.6e-5	1.8e8	1.9e-6
Embedded-ED	96 762 triangles	8648	53 379	5.3e-5	1.2e9	2.8e-7
Decomposition-ED	12 791 triangles	34 592	32 935	2.3e-4	5.2e10	6.4e-8
Decomposition-ED	36 331 triangles	34 592	45 172	1.7e-4	8.8e10	2.8e-8
Decomposition-ED (blocking)	922 triangles	34 592	26 520	2.7e-4	9.4e7	3.3e-8
Embedded-HD	1600 quads	112	1681	9.7e-4	1.6e5	1.3e-7
Embedded-HD	25 600 quads	448	25 921	4.3e-5	9.5e6	1.0e-7
Embedded-HD	102 400 quads	896	103 041	1.0e-5	7.6e7	9.8e-8
Embedded-ED (disconnected)	7596 triangles	12 052	4198	3.2e-4	2.0e6	6.1e-5
Embedded-ED (disconnected)	34 116 triangles	12 052	18 902	7.7e-5	4.1e7	4.0e-6
Embedded-ED (disconnected)	70 365 triangles	12 052	38 998	4.6e-5	2.6e8	8.9e-7
Embedded-HD (disconnected)	1600 quads	112	1681	8.5e-4	1.6e5	2.9e-7
Embedded-HD (disconnected)	25 600 quads	448	25 921	4.3e-5	9.6e6	2.3e-7
Embedded-HD (disconnected)	102 400 quads	896	103 041	1.0e-5	7.6e7	2.2e-7

Benchmark 1 (+3D): choice of Lagrange multiplier

Method	#-matr.	#-frac.	d.o.f.	nnz/size^2	$\|\cdot\|_2$-cond.
Box	1078 triangles	74	577	1.1e−2	2.2e3
TPFA	1386 triangles	95	1481	2.7e−3	4.8e4
MPFA	1348 triangles	91	1439	8.0e−3	5.8e4
EDFM	1369 quads	132	1501	3.3e−3	5.6e4
Flux-Mortar	1280 triangles	75	3366	1.8e−3	2.4e6
P-XFEM	961 quads	164	1650	8.0e−3	9.3e9
D-XFEM	1250 triangles	126	4474	1.3e−3	1.2e6
MFD	1 136 456 quads	38 600	2 352 280		
SLM-FEM: $\xi = 1000$	1089 quads	112	1374	–	1.3e5
LM-L^2	1089 quads	112	1374	6.7e−3	4.6e11
LM-L^2 - dual-Lagr.-Mult.	1089 quads	112	1156	9.7e−3	3.0e4
LM-L^2 - p0-Lagr.-Mult.	1089 quads	112	1377	6.3e−3	3.7e8
LM-L^2 - (3D)	35 937 hexas	3584	46 498	6.0e−4	7.7e12
LM-L^2 - dual-Lagr.-Mult. - (3D)	35 937 hexas	3584	39 304	1.4e−3	6.4e4
LM-L^2 - p0-Lagr.-Mult. - (3D)	35 937 hexas	3584	46 485	5.4e−4	1.7e11

High-resolution example

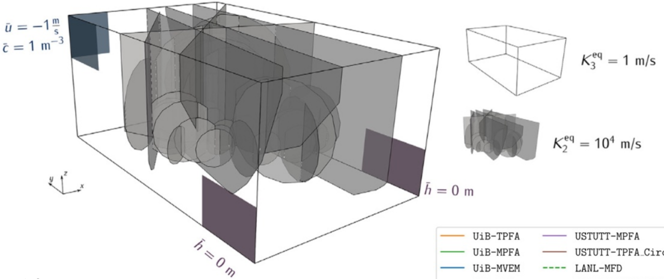

52 fractures

Matrix hydraulic conductivity K_3	$\boldsymbol{I}$	m/s
Fracture effective tangential hydraulic conductivity K_2	$1 \times 10^2 \boldsymbol{I}$	m³/s
Fracture effective normal hydraulic conductivity κ_2	2×10^6	1/s
Intersection effective tangential hydraulic conductivity K_1	1	m²/s
Intersection effective normal hydraulic conductivity κ_1	2×10^4	m/s
Matrix porosity ϕ_3	2×10^{-1}	
Fracture porosity ϕ_2	2×10^{-1}	
Intersection porosity ϕ_1	2×10^{-1}	
Fracture cross-sectional length ϵ_2	1×10^{-2}	m
Intersection cross-sectional area ϵ_1	1×10^{-4}	m²
Total simulation time	5×10^3	s
Time-step Δt	5×10^1	s

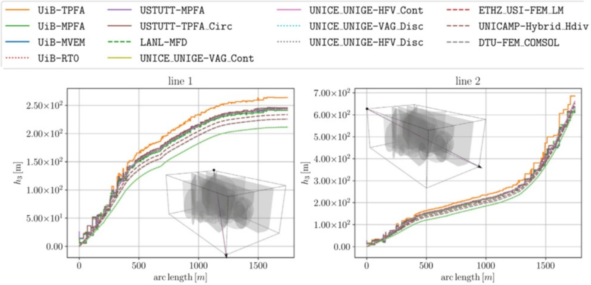

Matrix mesh: 62 676 992 tetrahedra

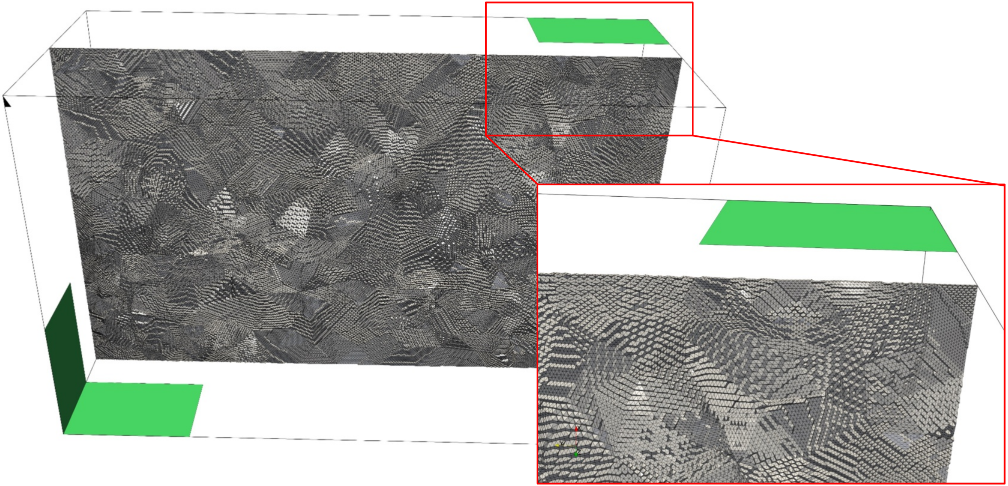

Fracture mesh: 3 367 552 triangles

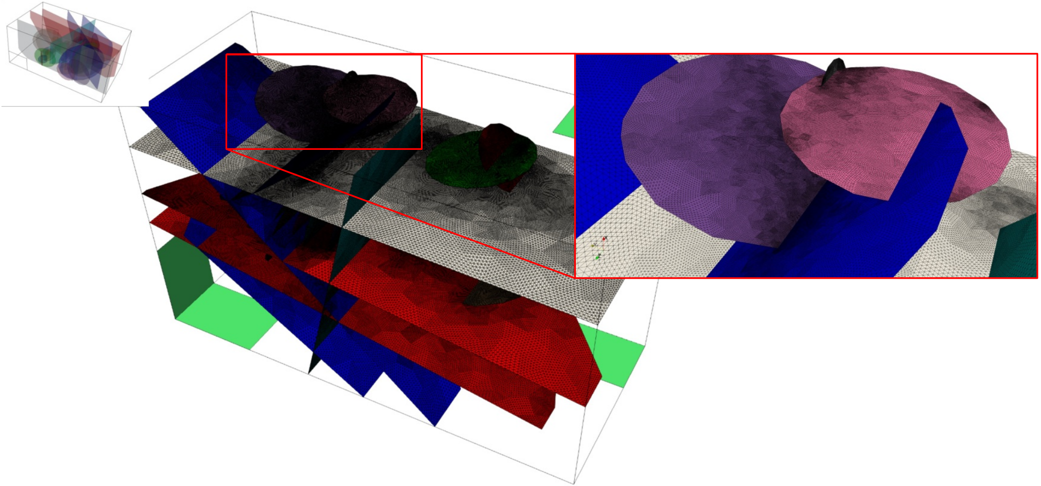

Flow: pressure iso-surfaces

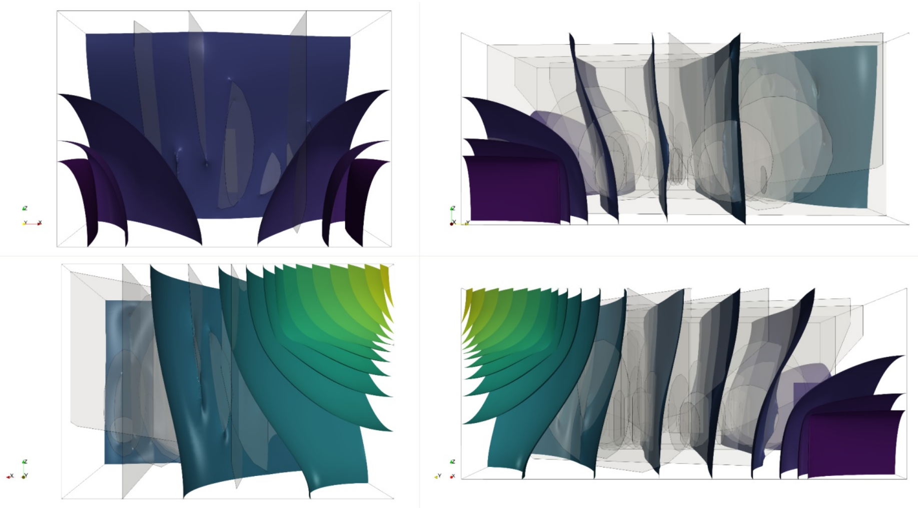

Flow: pressure iso-surfaces

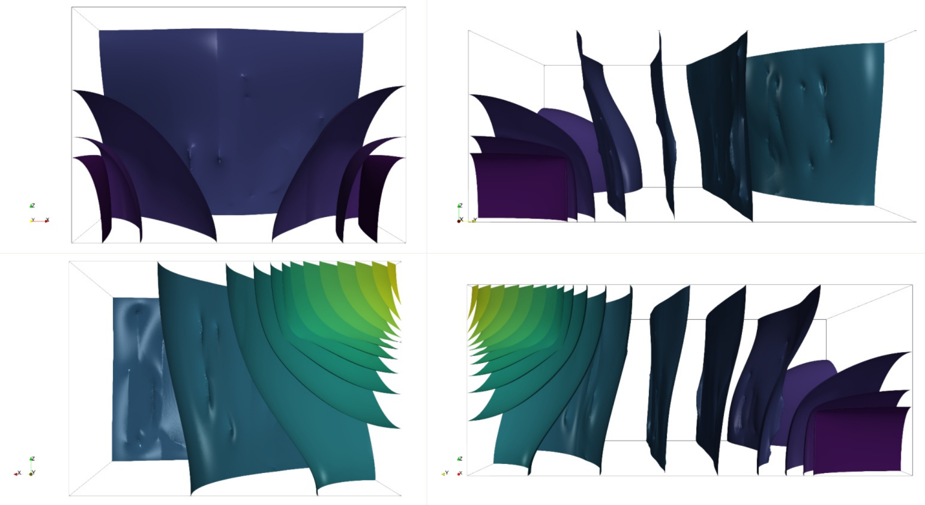

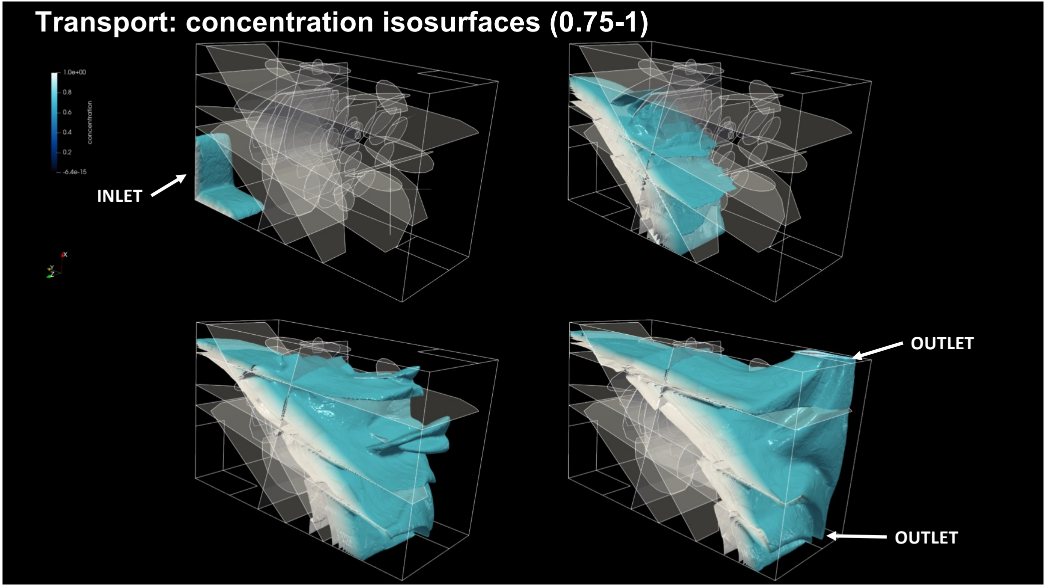
Transport: concentration isosurfaces (0.75-1)
1.0e+00
0.8
0.6
0.4
0.2
-6.4e-15
concentration
INLET
OUTLET
OUTLET

Similar idea for a more challenging scenario **Fluid-structure-contact interaction**

Project	Application	Fluid	Solid	Coupling	Contact	Article
AV-Flow	Heart-valves	FD	FEM	IB	-	Nestola et al. [2019]
-	Heart-valves	FEM	FEM	ID	Lagrange Multipliers (LM)	Nestola et al. [2021]
Fluya	Pumps	CVFEM	FEM	ID	Shifted-Penalty (SP)	In preparation

ID := Immersed Domain, IB := Immersed Boundary

FSI: Boundary-fitted methods

- **Matching boundary** of fluid and solid meshes
- Arbitrary Lagragian Eulerian (ALE)
- **Fluid mesh deforms** with solid mesh
- **Accurate** results at FSI interface
- Large displacements → **Distorted fluid grid** → reduced numerical stability and accuracy

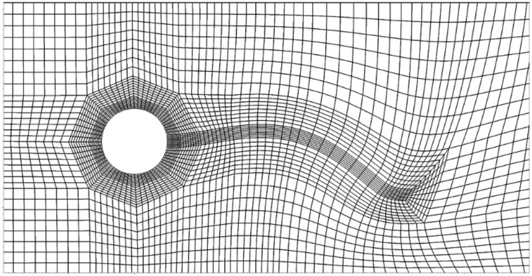

Figure: ALE mesh

FSI: Non Boundary-fitted fixed-grid methods

Immersed techniques

- **Independent meshes** of fluid and solid meshes
- Eulerian fluid formulation
- **Fuzzy** FSI interface → **higher resolution required** for reproducing accurate results
- **Flexible** choice of discretization for the fluid (*e.g.*, FEM, FVM, CVFEM, FDM) and software

Immersed domain → fluid and solid are **coupled in the** entire intersection **volume**

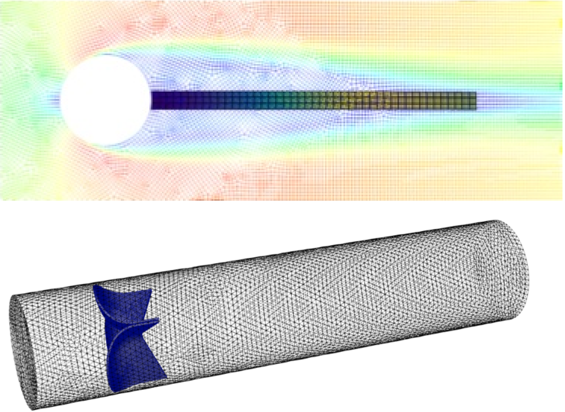

Figure: Super-imposed solid and fluid meshes

Glowinski et al. [1999], Baaijens [2001], Hesch et al. [2014]

Strong formulation of the fluid-structure-interaction problem

$$
\begin{aligned}
{}_f \frac{\partial \boldsymbol{u}_f}{\partial t} + {}_f (\boldsymbol{u}_f \cdot \nabla)\boldsymbol{u}_f + \boldsymbol{\sigma}_f - \boldsymbol{\lambda} &= \mathbf{0} \quad \text{in} \quad \Omega_f, \qquad \text{(Navier-Stokes equations)}\\
\nabla \cdot \boldsymbol{u}_f &= \mathbf{0} \quad \text{in} \quad \Omega_f,\\
{}_s \frac{\partial^2 \boldsymbol{\eta}_s}{\partial t^2} + \boldsymbol{\sigma}_s + \boldsymbol{\lambda} &= \mathbf{0} \quad \text{in} \quad \Omega_s(t), \qquad \text{(Elastodynamics equation)}\\
\frac{\partial \boldsymbol{\eta}_s}{\partial t} - \boldsymbol{u}_f &= \mathbf{0} \quad \text{in} \quad I = \Omega_f \cap \Omega_s(t),
\end{aligned}
$$

where
$\boldsymbol{u}_f$:= velocity, p_f := pressure, $\boldsymbol{\eta}_s$:= displacement, $\boldsymbol{\lambda}$:= Lagrange multiplier, := mass density, and initial and boundary conditions …

Contact between structures

- **Initial conditions for FSI simulation**
  - → Containment problem
  - → Large stresses in structure will cause interpenetration
- Cases with low resolution (TTS constraints)
- Multi-body contact and unilateral contact

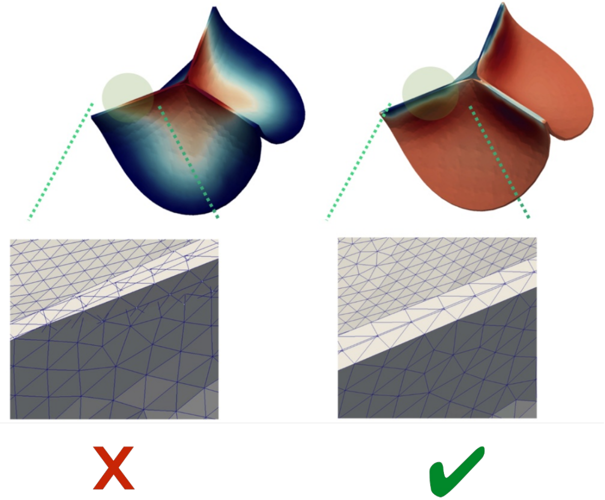

Dickopf and Krause [2009], Krause and Walloth [2012]

Two-body contact problem

- Elastic bodies $\Omega^m, \Omega^s \in \mathbb{R}^d$, $d \in \{2, 3\}$
- Lipschitz continuous boundaries ^{m}, ^{s}
- A priori unknown contact boundary $\partial\Omega_c = {}_c$
- Gap between the two bodies g_c

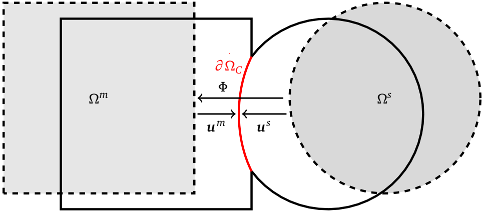

Contact conditions

- Smooth contact mapping: $\Phi : {}^{s}_{c} \longrightarrow {}^{m}_{c}$
- Vector field of normal directions: $\boldsymbol{n}_\Phi : {}^{s}_{c} \longrightarrow \mathbb{S}^2$

$$\boldsymbol{n}_\Phi(\boldsymbol{x}) = \begin{cases} \dfrac{\Phi(\boldsymbol{x}) - \boldsymbol{x}}{|\Phi(\boldsymbol{x}) - \boldsymbol{x}|}, & \text{if } \Phi(\boldsymbol{x}) \neq \boldsymbol{x}, \\ \boldsymbol{n}^s(\boldsymbol{x}), & \text{otherwise} \end{cases}$$

- Jump of the solution in $\boldsymbol{n}_\Phi$

$$[\![\boldsymbol{\eta}]\!] := \boldsymbol{\eta}^s - \boldsymbol{\eta}^m \circ \Phi \qquad [\![\ _n]\!] := [\![\boldsymbol{\eta}]\!] \cdot \boldsymbol{n}_\Phi$$

- Contact conditions

$$\left.\begin{array}{rll} \text{Non-penetration condition:} & [\![\ _n]\!] - g_c & \leqslant 0 \\ \text{Normal contact stress:} & p_n(\boldsymbol{\eta}^s) & \leqslant 0 \\ \text{Complementary condition:} & ([\![\ _n]\!] - g_c) p_n(\boldsymbol{\eta}^s) & = 0 \\ \text{Tangential contact stress:} & \boldsymbol{\tau}_t(\boldsymbol{\eta}^s) & = 0 \end{array}\right\} \text{ on } \ _c$$

FSCI problem discretization

- FEM for the structure
- CVFEM[a] for the fluid
- Variants of mortar-method[b] for the coupling between fluid and structure
- $\frac{\partial \eta_s}{\partial t} - \boldsymbol{u}_f = \mathbf{0} \rightarrow \int_I \left(\sum_i \frac{\partial \ _i}{\partial t} \varphi_i - \sum_j u_j \boldsymbol{\theta}_j \right) \cdot \mu_k = 0 \quad \forall \mu_k \in \Lambda$ (weak equality condition)
- Where $\varphi_i \in \boldsymbol{V}_s, \boldsymbol{\theta}_j \in \boldsymbol{V}_f, \mu_k \in \Lambda$ are the basis functions for structure, fluid, and multiplier discretizations, respectively
- Similary for contact

[a] Baliga and Patankar [1983]

[b] Bernardi et al. [2005]

Lagrange multiplier

Standard interpolation (*etc.*)

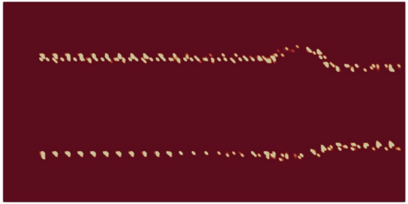

Variational approach

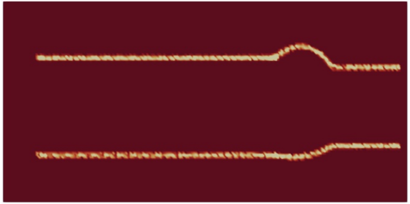

Parallel coupling procedure

Coupling types

- FSI Volumetric coupling
- Contact conditions Surface coupling

Geometric operations

- Structure considered in the **deformed configuration**
- Intersection mesh for numerical quadrature of the coupling conditions fluid-structure and structure-structure

Krause and Zulian [2016]

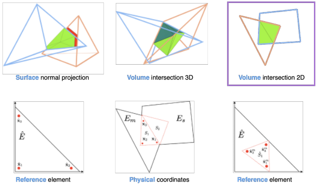

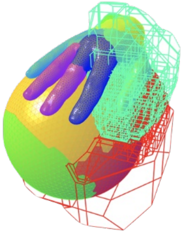

Bio-prosthetic heart-valve simulation

Spatial discretization

- Fluid: FEM (+SUPG), with the MOOSE framework [Peterson et al., 2018]
- Structure: FEM

Time discretization

- Fluid: Backward Differentiation Formula (BDF2)
- Structure: Contact-stabilized-Newmark scheme [Krause and Walloth, 2012]

Staggered approach

- Fluid and structure sub-problems solved separately within a Picard iteration
- A multibody contact problem is solved with a non-smooth sub-structuring method[a]

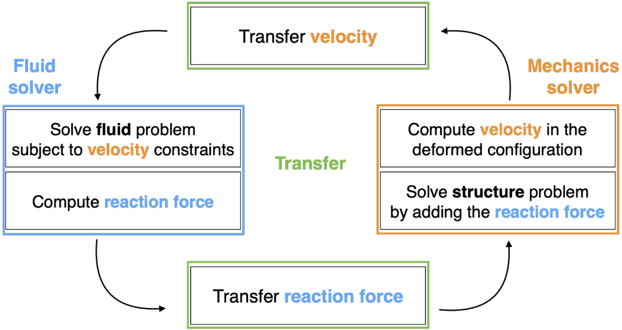

[a] Article is work in progress

Bio-prosthetic heart-valve simulation

Aortic valve stenosis

- Prevalent valvular pathology in Western countries
- Progressive thickening of the valve
- Results in severe impairment of the valve motion → Replacement with bioprosthetic valve

Bioprosthetic heart valve

- Limited durability
- Numerical simulations for studying valve design

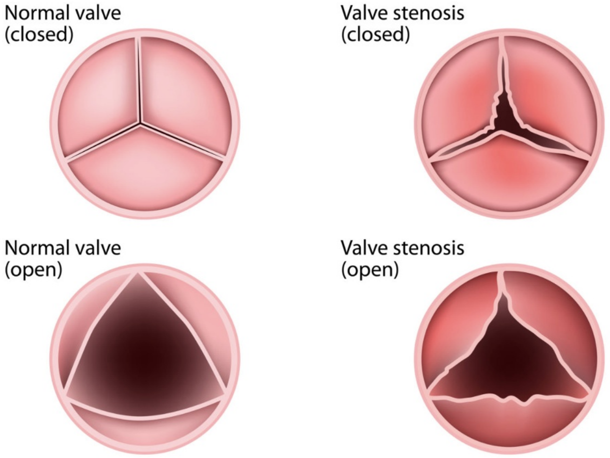

Bio-prosthetic heart-valve simulation

BHV model

- **Holzapfel fiber-reinforced material**
- Two valve designs
- with and without fibers

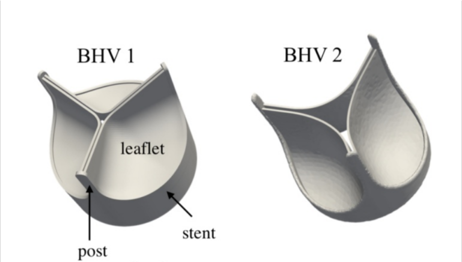

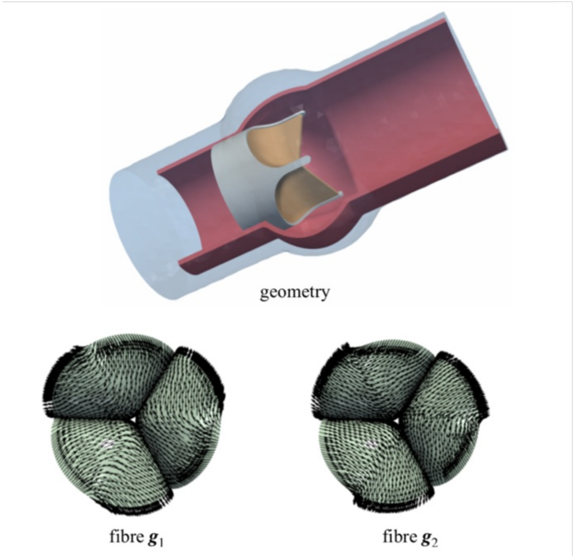

Bio-prosthetic heart-valve simulation

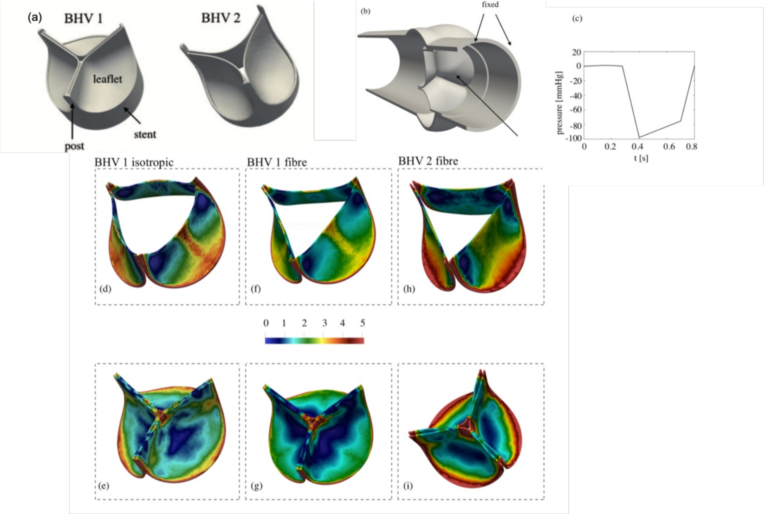

Purely structure simulation of the BHV

- Pressure profile imposed on the structure
- VonMises stresses are lower in the fiber-reinforced BHV 1 model

Bio-prosthetic heart-valve simulation

Fiber reinforced BHV 1 performance

- Mechanical and haemodynamic performance
- (a) Velocity. Inflow boundary condition.
- (b) Windkessel model for pressure gradient between 80 and 120 mmHg
- (c) Systole
- (d) Diastole

More details in Nestola, Zulian, Gaedke-Merzhäuser, and Krause [2021]

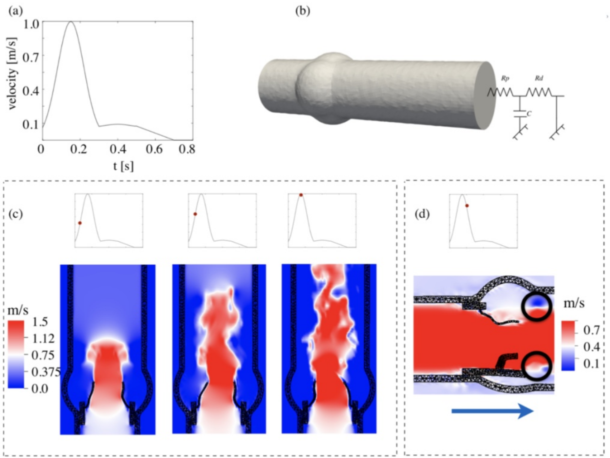

FSCI: Challenges in fluid-structure-contact interaction

- Properly and efficiently simulating the sub-problems is challenging on their own
- **Complex setups and geometries** → generality and robustness of methods and algorithms
  - Non-smooth interactions between structures due to **contact**
  - Closing gaps and **blockage** of fluid flow
  - From CAD models to proper initial value problem
  - Physical parameters and engineering goals
  - **FP70 Video**
- **Transient simulation (3 + 1)D** → scalable solution techniques and high-performance codes
  - Simulation time is constrained by business goals and computational resources
  - Sufficient fidelity vs computational effort
- (Limited freedom due to split development efforts)

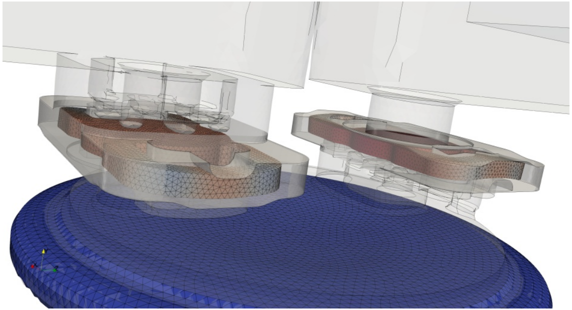

Figure: Set-up for FSCI in idealized hydro-pump

Hydro-pump simulation

Simulation of fluid-structure interaction in diaphragm pumps

- Collaboration with **HSLU**, article is WIP
- Structure only IVP initialization
- NeoHookean hyperelastic material
- Monolithic formulation

Spatial discretization

- Fluid: CVFEM
- Structure: FEM

Time discretization

- Fluid: Implicit Euler
- Structure: Newmark scheme

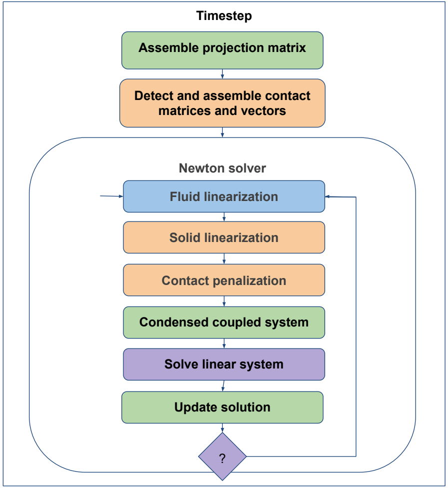

Hydro-pump simulation

FSI Saddle-point system (after linearization)

$$\begin{vmatrix} \mathbf{A}_f & \mathbf{0} & -\mathbf{B}^T \\ \mathbf{0} & \mathbf{A}_s & \mathbf{D}^T \\ -\mathbf{B} & \mathbf{D} & \mathbf{0} \end{vmatrix} \begin{vmatrix} \mathbf{u}_f \\ \mathbf{u}_s \\ \boldsymbol{\lambda} \end{vmatrix} = \begin{vmatrix} \mathbf{R}_f \\ \mathbf{R}_s \\ \mathbf{R}_{\mathrm{FSI}} \end{vmatrix},$$

with dual-Lagrange multipliers

$$\mathbf{T} = \mathbf{D}^{-1}\mathbf{B}, \quad \mathbf{u}_s = \mathbf{D}^{-1}\mathbf{R}_{\mathrm{FSI}} + \mathbf{T}\;\;\mathbf{u}_f,$$

$$\boldsymbol{\lambda} = \mathbf{D}^{-T}\left(\mathbf{R}_s - \mathbf{A}_s(\mathbf{D}^{-1}\mathbf{R}_{\mathrm{FSI}} + \mathbf{T}\;\;\mathbf{u}_f)\right),$$

we compute (Gaussian elimination on paper)

$$(\mathbf{A}_f + \mathbf{T}^T\mathbf{A}_s\mathbf{T})\;\;\mathbf{u}_f = \mathbf{R}_f + \mathbf{T}^T\mathbf{R}_s - \mathbf{T}^T\mathbf{A}_s\mathbf{D}^{-1}\mathbf{R}_{\mathrm{FSI}},$$

where $\mathbf{R}_{\mathrm{FSI}} = -(\mathbf{D}\mathbf{u}_s{}^k - \mathbf{B}\mathbf{u}_f{}^k)$.

Hydro-pump simulation

- Condensed linearized system (k) is solved for the velocity increment $\mathbf{u}_f$
- Structure equations adapted after linearization
  - $\mathbf{A}_s = \frac{2}{\,}\mathbf{M}_s + \frac{\,}{2}\mathbf{H}_s(\boldsymbol{\eta}_s{}^k)$,
  - $\mathbf{R}_s = \boldsymbol{f}_s{}^{\text{external}} - \boldsymbol{f}_s{}^{\text{contact}} - \boldsymbol{f}_s{}^{\text{int}}(\boldsymbol{\eta}_s{}^k) + \mathbf{M}_s\left(\mathbf{a}_s{}^t - \frac{2}{\,}(\mathbf{u}_s{}^k - \mathbf{u}_s{}^t)\right)$,
  - after solve $\mathbf{u}_s{}^{k+1} = \mathbf{u}_s{}^k + \mathbf{T}\ \ \mathbf{u}_f - (\mathbf{u}_s{}^k - \mathbf{T}\mathbf{u}_f{}^k)$,
  - t := time, := time-step.
- The structure displacement is computed with $\boldsymbol{\eta}_s{}^{t+1} = \boldsymbol{\eta}_s{}^t + \frac{\,}{2}(\mathbf{u}_s{}^t + \mathbf{u}_s{}^{t+1})$,
- Penalty methods for $\boldsymbol{f}_s{}^{\text{contact}}$
  - Interior penalty, logarithmic barrier (or polynomial)
  - **Exterior penalty** and **shifted** variant (*Augmented Lagrangian*)

Hydro-pump simulation

Shifted-penalty method[a]

- Classical penalty term in the objective is modified (augmented Lagrangian) $\frac{1}{2}\ g_c^2 \rightarrow \frac{1}{2}\ (s + g_c)^2$
- The shift s is used to "change the obstacle"
- Same penalty parameter but better enforcement of non-penetration condition
- The contribution included in the FSI by means of f_s^{contact} (details not shown here)

[a] Divi and Kesavan [1982], Zavarise [2015]

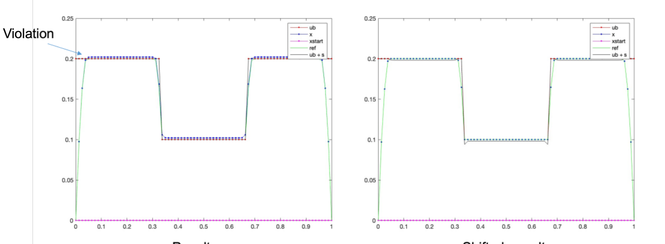

Penalty   Shifted-penalty

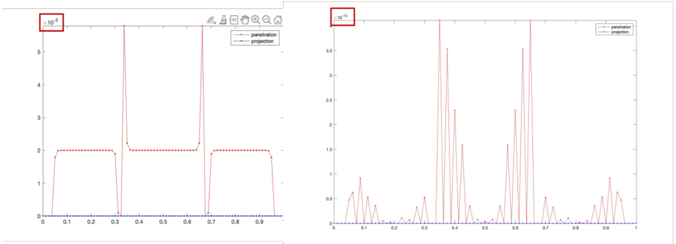

Penalty
(penetration ~ 1e-3)

Shifted-penalty
(penetration ~ 1e-13)

Hydro-pump: initial conditions

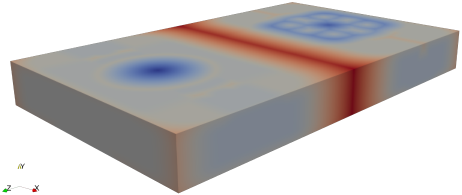

1) SDF on structured grid

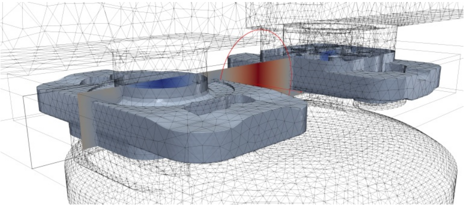

2) In small volume w.r.t. the fluid domain

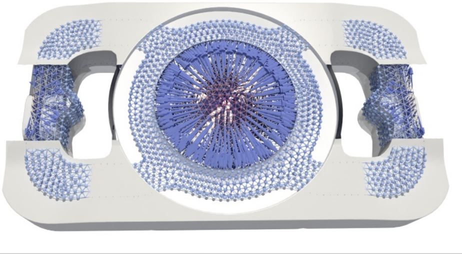

3) SDF is resampled to solid mesh

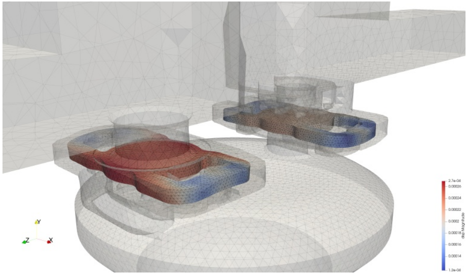

4) Contact problem solved (3 + 4) until contained

Hydro-pump simulation: simplified diaphragm pump

Simplified diaphragm pump test-rig

1. Rigid driving piston
2. Fluid reservoir
3. Valve limiters
4. Valves[a]
5. Transparent plexiglass window

[a] Parts removed due to copyright

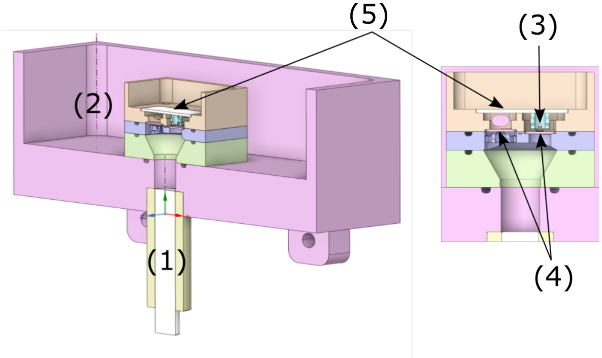

Hydro-pump simulation: simplified diaphragm pump

Simplified diaphragm pump mesh

- Fluid 122 432 nodes (637 570 cells)
- Structure 11 140 nodes (47 045 cells)

Simulation setup

- Rigid piston modelled as inlet/outlet boundary with prescribed transient flow signal
- Water surface of reservoir modelled as opening with constant static pressure
- Valves modelled as immersed structures, anchored through contact with fluid domain walls

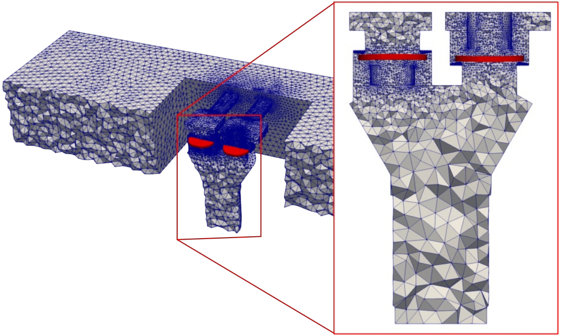

Hydro-pump simulation: simplified diaphragm pump

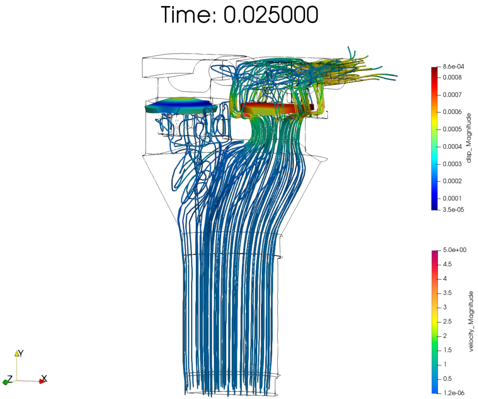

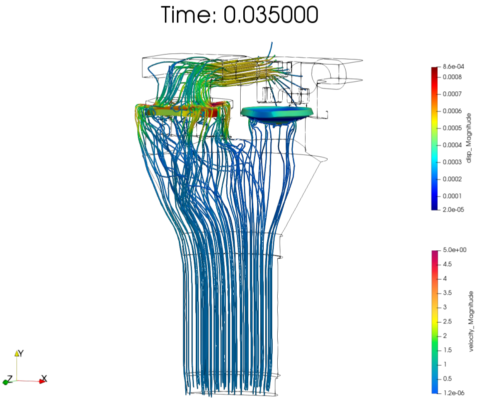

Flow from the piston cylinder into the water reservoir during the pressure stroke

Flow from the water reservoir into the piston cylinder during the suction stroke

Hydro-pump simulation: simplified diaphragm pump

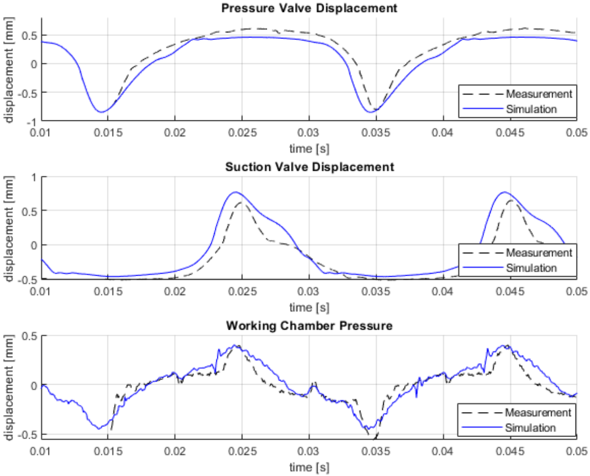

On the role of aortic valve architecture for physiological hemodynamics and valve replacement

Work from

- Corso and Obrist [2024a]
- Corso and Obrist [2024b]
- Tsolaki, Corso, Zboray, Avaro, Appel, Liebi, Bertazzo, Heinisch, Carrel, Obrist, et al. [2023]
- Corso, Coulter, and Nestola [2024]
- Based on AVFLOW [Nestola, Becsek, Zolfaghari, Zulian, De Marinis, Krause, and Obrist, 2019]
- Videos are courtesy of Pascal Corso (ETHZ)

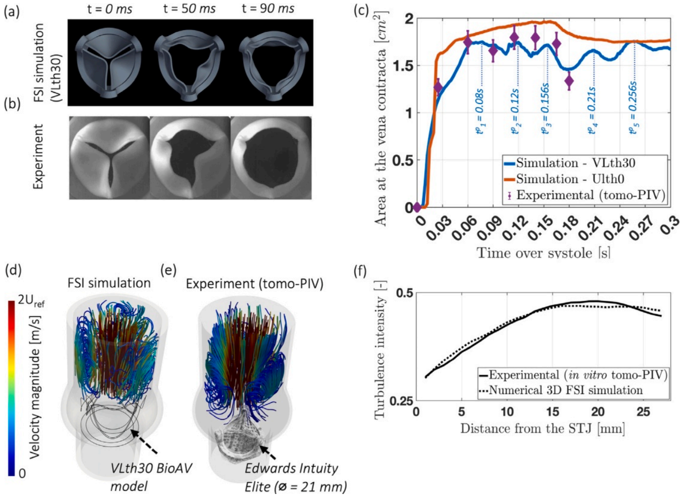

Contact between rough surfaces using a dual mortar method

- Work from von Planta, Vogler, Zulian, Saar, and Krause [2020]

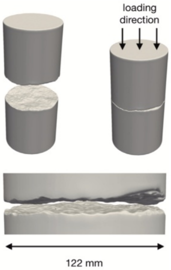

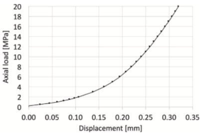

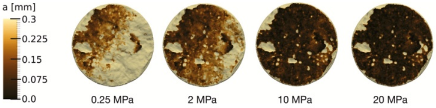

Fig. 6. View of the different aperture fields under increasing confining stresses of 0.25, 2, 10 and 20 MPa.

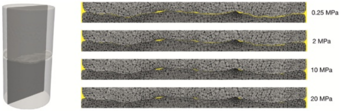

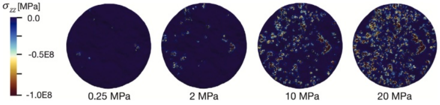

Fig. 8. Top view of the lower fracture surface for confining stresses of 2, 10 and 20 MPa. The color indicates the vertical stresses σ_{zz}.

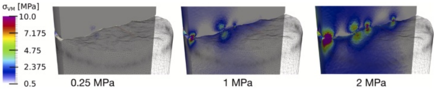

Fig. 9. The color indicates von Mises stresses around contact points during the closure of the fracture at confining stresses of 0.25, 1 and 2 MPa.

Scalable hierarchical PDE sampler for generating spatially correlated random fields using nonmatching meshes

- Work from Osborn, Zulian, Benson, Villa, Krause, and Vassilevski [2018]
- Based on Krause and Zulian [2016] integrated in MFEM

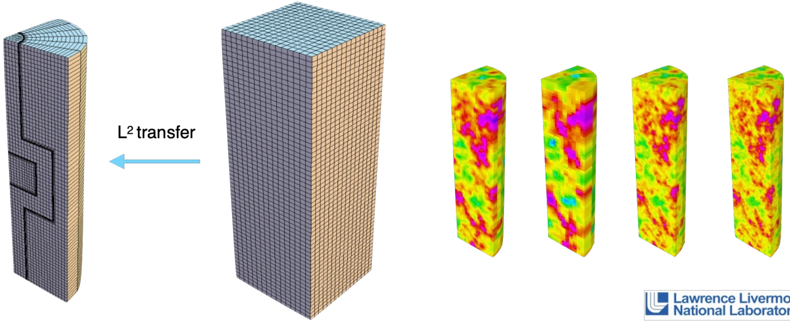

Crooked pipe problem   Extended domain mesh   Hierarchical sampling with MLMC

Lawrence Livermore National Laboratory

Preliminary work on semi-structured operators

- Greater spatio-temporal resolution of simulations needed to capture relevant small scale dynamics
- More complex physics such as multi-phase flows
- Supercomputing mandatory → Semi-structured operators
- PASC project 2025-2028 XSES-FSI (`https://pasc-ch.org/index.html`)

Comparison with cuSPARSE on NVIDIA P100 (FP64: 4.7 TFlop/s)

Throughput in MDoF/s (Million degrees of freedom per second)

- **Matrix-Free** (MF) operators achieve higher throughput than cuSPARSE SpMV except **tet4** (highest macrotet4)
- **Laplacian**: **1.8x** and **3.2x** speedup over **SpMV** and **tet4**, respectively
- **Linear Elasticity**: **3.4x** and **2.9x** speedup over **SpMV** and **tet4**, respectively
- **In line with results from ECP, additional regularity benefits performance**

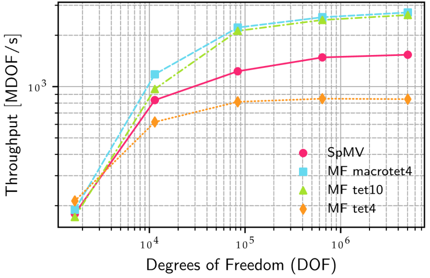

Laplacian

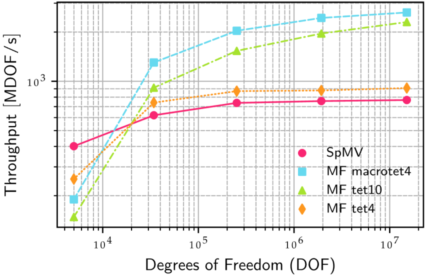

Linear elasticity

Memory footprint **from structured to unstructured**

Basic example

- Cuboid with $\Omega = (0,2) \times (0,1) \times (0,1)$
- $80 \times 40^2 \times 8^3 = 65\,536\,000$ elements, and $66\,049\,281$ nodes.
- **Semi-structured mesh** ("level 8"), with $128\,000$ macro-elements.
- Laplace operator stored with **first-fundamental form**, i.e., 6 scalars per element (*FP16*)
- Nodal field (*FP64*), Elemental indices (*INT32*), Coordinates (*FP32*)

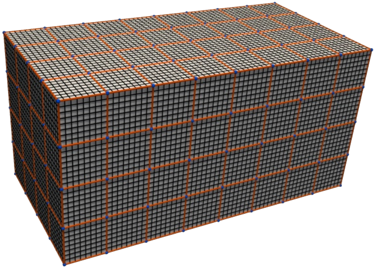

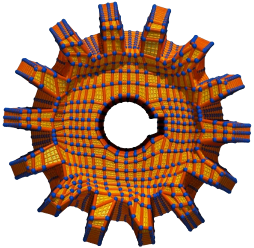

Mesh	Points [GB]	Elements [GB]	Field [GB]	Operator [GB]	Total [GB]	Proportion
Structured	0	0	0.528	0	0.528	1
Semi-structured (8)	0.001	**0.37**	0.528	**0.0015**	0.9	**1.7**
Unstructured	0.79	2	0.528	0.7864	4.1	**7.7**

Compromise between convenience and regularity

- Complex mesh descriptions → **Boundary parametrization** [Zulian et al., 2017] (**to be revisited**)
- Memory efficiency and bandwidth requirements
- **Implicit** hierarchical **structure** to be mapped to compute hardware
- Geometric **multigrid** methods and **sub-structuring** methods
- Workload granularity (1 element per thread to 1 element per GPU)
- Main target is solution strategies employing **matrix-free** operators
- Performance of linear operators might be further improved by exploting stencils

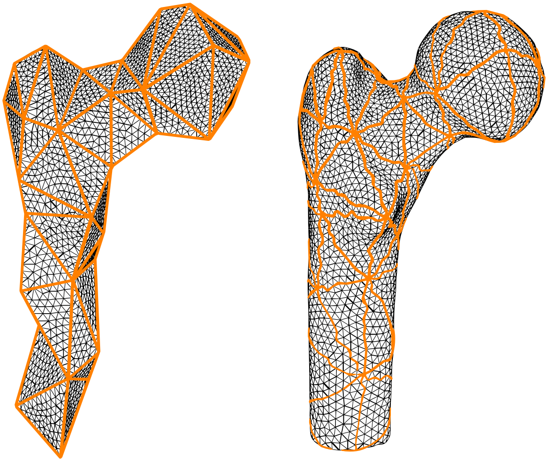

Performance of semi-structured operators

Throughput in MDoF/s (Million degrees of freedom per second)

- **Baseline** Laplace operator for geometric multigrid
- **#nodes per element** is $(N+1)^3$
- Factor of 8 increase in elements does not translate to 8x larger compute times
- Finer levels have higher throughput approx. **3-5x**
- On **NVIDIA H100 GPU** best throughput **20320.3** [MDOF/s]
- On **Mac M1 Max** (8 OpenMP threads) best throughput **758.631** [MDOF/s] ($N = 10$)
- On **Shaheen's AMD EPYC 9654**, perf. limited by basic OpenMP parallelization (0.5-0.6 efficiency), for Level = 16 **#elements 1 943 764 992**, **#nodes 1 948 441 249**

Table: One node on Shaheen: **192 OpenMP threads**. Coarse mesh ($N = 1$) #elements 78^3, approx. 1.9 G dofs

N	TTS [s]	Throughput [MDOF/s]
16	0.303056	6429.3
8	0.0390528	6251.56
4	0.00781309	3924.73
2	0.000913524	4236.23
1	0.000239933	2054.9

Solution to contact problems with semi-structured matrix-free finite elements operators[1]

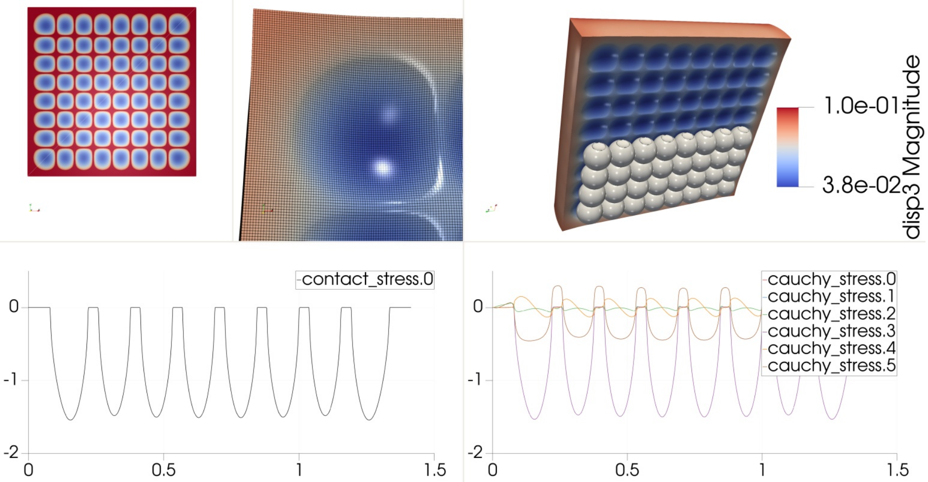

[1] Collaboration with PSU for algebraic coarse spaces. Article in preparation.

High-frequency surface geometric features

- Geometric MG proof-of-concept for **Fluya FSCI**
- Unilateral linearized contact problem, SDF obstacle
- **WIP**: baseline implementation to be optimized
- One Shaheen III node, AMD EPYC 9654 **CPUs** (192 cores)
- TLP: OpenMP
- **#elements** 136 294 400 (HEX8)
- **#nodes** 137 380 497 → **#dofs** 412 141 491
- Matrix-based version does not fit one node
- Time-to-solution: **39 minutes**
- 65% **Linear-elasticity operator**
- 82% **Nonlinear smoothing** → **#steps** 7230
  fine-level block-Jacobi (block size $= 3 \times 3$)

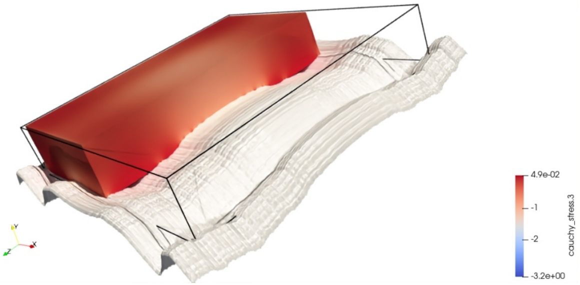

WIP: Shifted-Penalty Multigrid for Contact

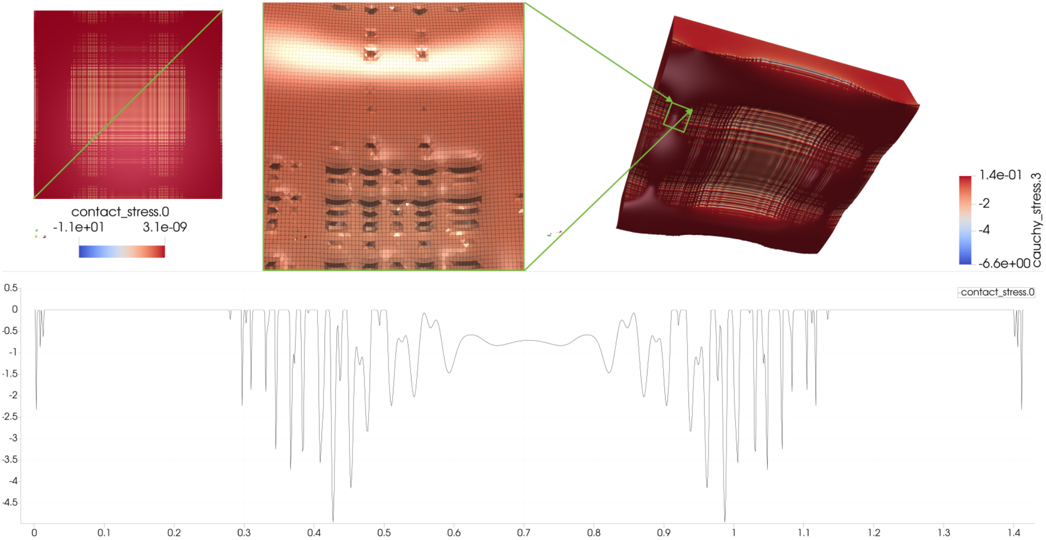

Resampling: structured → unstructured

- Approximate numerical quadrature
- Sampling a field defined over a structured grid for each quadrature node in the **tetrahedral** mesh.
- **Gather memory access pattern**
- First and second order iso-parametric mesh
- We start from structured to unstructured, we will address semi-structured to semi-structured later
- Effects of approximate quadrature? (study by Boffi, Credali, and Gastaldi [2024])
- Preliminary work in collaboration with Simone Riva (USI)

Example for a triangular mesh: quadrature-points for a triangle, nodes of the structured grid

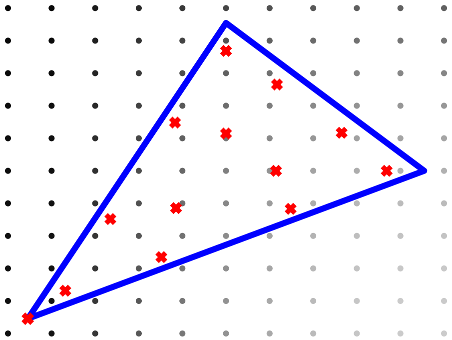

Performance results **Linear TET4 elements** (CPU)

AMD EPYC 9654 96-Core on Shaheen III, KAUST Supercomputer

$21 \cdot 10^6$ tetrahedral elements, $900 \times 900 \times 900$ structured mesh

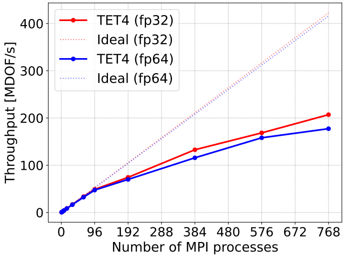

Degree of Freedom / s

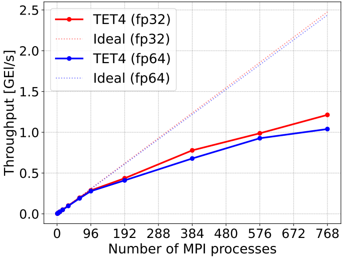

Elements / s

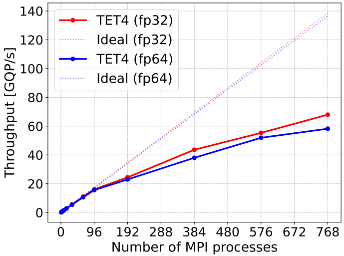

Quadrature points / s

- 10 nodes per element, and 56 quadrature points per element

Performance results **Quadratic TET10 elements** (CPU)

AMD EPYC 9654 96-Core on Shaheen III, KAUST Supercomputer

$21 \cdot 10^6$ tetrahedral elements, $900 \times 900 \times 900$ structured mesh

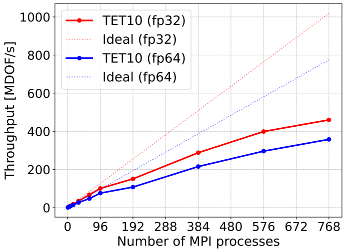

Degree of Freedom / s

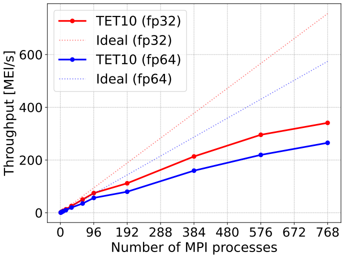

Elements / s

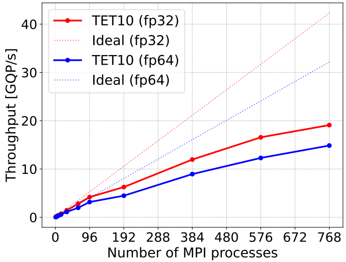

Quadrature points / s

- 10 nodes per element, and 56 quadrature points per element

CUDA Tiled-partitioned quadrature (GPU)

- A tile consists of a subset of a Warp (32 lanes) of a GPU vector unit, and each GPU thread occupies one lane
- One tetrahedral element per tile
- The performances significantly change as a function of the tile size *N*

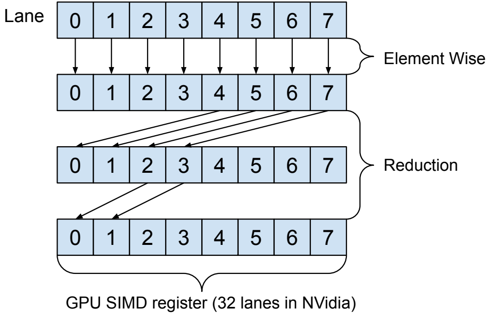

Performance results **Quadratic TET10 elements** (GPU)

GH200 nodes @ Alps CSCS

$21 \cdot 10^6$ tetrahedral elements, $900 \times 900 \times 900$ structured mesh

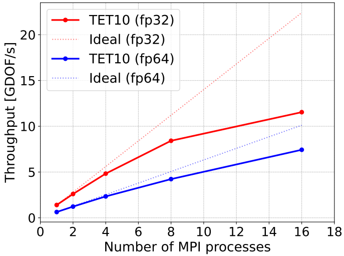

M Degree of Freedom / s

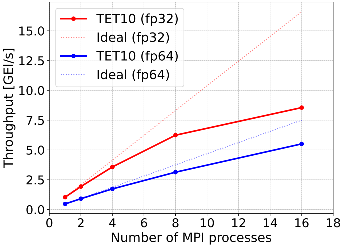

M Elements / s

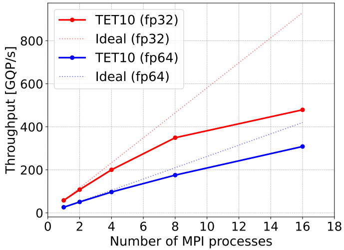

G Quadrature points / s

- 10 nodes per element, and 56 quadrature points per element

Conclusions

Thank you for your attention!

Summary

- Immersed approach to flow in fractured porous media and FSI
- Example numerical applications
- Open-source libraries (BSD 3-clause license)
  - `https://github.com/mfem/mfem` (branch “moonolith_h1_bugfix” PR in review)
  - `https://bitbucket.org/zulianp/utopia`
  - `https://bitbucket.org/zulianp/par_moonolith`

Future work

- Focus on FSCI models and large scale FSI and FSCI
- Hybrid matrix-free and matrix-based algorithm on GPU
- Preconditioning techniques exploiting semi-structured operators
- ...

Acknowledgments

- Innosuisse project 48321.1 IP-ENG
- Swiss National Fund (SNF)
  - Immersed methods for fluid-structure-contact-interaction simulations and complex geometries
  - Stress-based methods for variational inequalities in Solid Mechanics
- UniDistance Suisse and USI-FIR
- PASC 2025-2028 – XSES-FSI

Connect

Frank P. T. Baaijens. A fictitious domain/mortar element method for fluid–structure interaction. *International Journal for Numerical Methods in Fluids*, 35(7):743–761, 2001. doi: 10.1002/1097-0363(20010415)35:7<743::AID-FLD109>3.0.CO;2-A.

BR Baliga and SV Patankar. A control volume finite-element method for two-dimensional fluid flow and heat transfer. *Numerical Heat Transfer*, 6(3):245–261, 1983.

Christine Bernardi, Yvon Maday, and Francesca Rapetti. Basics and some applications of the mortar element method. *GAMM-Mitteilungen*, 28(2):97–123, 2005.

Daniele Boffi, Fabio Credali, and Lucia Gastaldi. Quadrature error estimates on non-matching grids in a fictitious domain framework for fluid-structure interaction problems. *arXiv preprint arXiv:2406.03981*, 2024.

P. Corso, F. B. Coulter, and M. G. Nestola. How do polymeric aortic valves perform? a computational study of blood-structure dynamics under various material and geometrical conditions. In *1st European Fluid Dynamics Conference*, Aachen, Germany, 2024.

Pascal Corso and Dominik Obrist. On the role of aortic valve architecture for physiological hemodynamics and valve replacement, part i: Flow configuration and vortex dynamics. *Computers in biology and medicine*, 176:108526, 2024a.

Pascal Corso and Dominik Obrist. On the role of aortic valve architecture for physiological hemodynamics and valve replacement, part ii: Spectral analysis and anisotropy. *Computers in biology and medicine*, 176:108552, 2024b.

Thomas Dickopf and Rolf Krause. Efficient simulation of multi-body contact problems on complex geometries: a flexible decomposition approach using constrained minimization. *International journal for numerical methods in engineering*, 77(13): 1834–1862, 2009.

R Divi and HK Kesavan. A shifted penalty function approach for optimal load-flow. *IEEE transactions on power apparatus and systems*, (9):3502–3512, 1982.

R. Glowinski, T.-W. Pan, T.I. Hesla, and D.D. Joseph. A distributed lagrange multiplier/fictitious domain method for particulate flows. *International Journal of Multiphase Flow*, 25(5):755 – 794, 1999. ISSN 0301-9322. doi: https://doi.org/10.1016/S0301-9322(98)00048-2. URL `http://www.sciencedirect.com/science/article/pii/S0301932298000482`.

C Hesch, AJ Gil, A Arranz Carreño, J Bonet, and P Betsch. A mortar approach for fluid–structure interaction problems: Immersed strategies for deformable and rigid bodies. *Comput. Method Appl. M.*, 278:853–882, 2014.

Rolf Krause and Mirjam Walloth. Presentation and comparison of selected algorithms for dynamic contact based on the newmark scheme. *Applied Numerical Mathematics*, 62(10):1393–1410, 2012.

Rolf Krause and Patrick Zulian. A parallel approach to the variational transfer of discrete fields between arbitrarily distributed unstructured finite element meshes. *SIAM Journal on Scientific Computing*, 38(3):C307–C333, 2016. doi: 10.1137/15M1008361. URL `https://epubs.siam.org/doi/10.1137/15M1008361`.

Maria G C Nestola, Patrick Zulian, Lisa Gaedke-Merzhäuser, and Rolf Krause. Fully coupled dynamic simulations of bioprosthetic aortic valves based on an embedded strategy for fluid–structure interaction with contact. *EP Europace*, 23(Supplement_1): i96–i104, 03 2021. ISSN 1099-5129. doi: 10.1093/europace/euaa398. URL `https://doi.org/10.1093/europace/euaa398`.

Maria Giuseppina Chiara Nestola, Barna Becsek, Hadi Zolfaghari, Patrick Zulian, Dario De Marinis, Rolf Krause, and Dominik Obrist. An immersed boundary method for fluid-structure interaction based on variational transfer. *Journal of Computational Physics*, 398:108884, 2019. ISSN 0021-9991. doi: https://doi.org/10.1016/j.jcp.2019.108884. URL `http://www.sciencedirect.com/science/article/pii/S0021999119305820`.

Sarah Osborn, Patrick Zulian, Thomas Benson, Umberto Villa, Rolf Krause, and Panayot S Vassilevski. Scalable hierarchical PDE sampler for generating spatially correlated random fields using nonmatching meshes. *Numerical Linear Algebra with*

Applications, 25(3):e2146, 2018. doi: 10.1002/nla.2146. URL
`https://onlinelibrary.wiley.com/doi/abs/10.1002/nla.2146`.

John W Peterson, Alexander D Lindsay, and Fande Kong. Overview of the incompressible navier–stokes simulation capabilities in the moose framework. *Advances in Engineering Software*, 119:68–92, 2018.

Philipp Schädle, Patrick Zulian, Daniel Vogler, Sthavishtha R Bhopalam, Maria GC Nestola, Anozie Ebigbo, Rolf Krause, and Martin O Saar. 3d non-conforming mesh model for flow in fractured porous media using lagrange multipliers. *Computers & Geosciences*, 132:42–55, 2019.

Elena Tsolaki, Pascal Corso, Robert Zboray, Jonathan Avaro, Christian Appel, Marianne Liebi, Sergio Bertazzo, Paul Philipp Heinisch, Thierry Carrel, Dominik Obrist, et al. Multiscale multimodal characterization and simulation of structural alterations in failed bioprosthetic heart valves. *Acta biomaterialia*, 169:138–154, 2023.

Cyrill von Planta, Daniel Vogler, Patrick Zulian, Martin O. Saar, and Rolf Krause. Contact between rough rock surfaces using a dual mortar method. *International Journal of Rock Mechanics and Mining Sciences*, 133:104414, 2020. ISSN 1365-1609. doi: https://doi.org/10.1016/j.ijrmms.2020.104414. URL
`http://www.sciencedirect.com/science/article/pii/S1365160919308688`.

Giorgio Zavarise. The shifted penalty method. *Computational Mechanics*, 56:1–17, 2015.

Patrick Zulian, Philipp Schädle, Liudmila Karagyaur, and Maria Nestola. Comparison and application of non-conforming mesh models for flow in fractured porous media using dual Lagrange multipliers, 2020.

Patrick Zulian, Teseo Schneider, Kai Hormann, and Rolf Krause. Parametric finite elements with bijective mappings. *BIT Numerical Mathematics*, 57(4):1185–1203, dec 2017. ISSN 1572-9125. doi: 10.1007/s10543-017-0669-6. URL
`https://doi.org/10.1007/s10543-017-0669-6`.